

# Measurement of the inclusive semileptonic branching fraction of $B$ mesons and $|V_{cb}|$

(The Belle Collaboration)

K. Abe<sup>9</sup>, K. Abe<sup>44</sup>, T. Abe<sup>45</sup>, I. Adachi<sup>9</sup>, Byoung Sup Ahn<sup>16</sup>, H. Aihara<sup>46</sup>, M. Akatsu<sup>23</sup>,  
 Y. Asano<sup>51</sup>, T. Aso<sup>50</sup>, V. Aulchenko<sup>2</sup>, T. Aushev<sup>13</sup>, A. M. Bakich<sup>41</sup>, Y. Ban<sup>34</sup>, E. Banas<sup>28</sup>,  
 A. Bay<sup>19</sup>, I. Bedny<sup>2</sup>, P. K. Behera<sup>52</sup>, A. Bondar<sup>2</sup>, A. Bozek<sup>28</sup>, M. Bračko<sup>21,14</sup>,  
 J. Brodzicka<sup>28</sup>, T. E. Browder<sup>8</sup>, B. C. K. Casey<sup>8</sup>, P. Chang<sup>27</sup>, Y. Chao<sup>27</sup>, B. G. Cheon<sup>40</sup>,  
 R. Chistov<sup>13</sup>, S.-K. Choi<sup>7</sup>, Y. Choi<sup>40</sup>, M. Danilov<sup>13</sup>, L. Y. Dong<sup>11</sup>, A. Drutskoy<sup>13</sup>,  
 S. Eidelman<sup>2</sup>, V. Eiges<sup>13</sup>, Y. Enari<sup>23</sup>, F. Fang<sup>8</sup>, C. Fukunaga<sup>48</sup>, N. Gabyshev<sup>9</sup>,  
 A. Garmash<sup>2,9</sup>, T. Gershon<sup>9</sup>, B. Golob<sup>20,14</sup>, K. Gotow<sup>53</sup>, R. Guo<sup>25</sup>, K. Hanagaki<sup>35</sup>,  
 F. Handa<sup>45</sup>, K. Hara<sup>32</sup>, T. Hara<sup>32</sup>, N. C. Hastings<sup>22</sup>, H. Hayashi<sup>24</sup>, M. Hazumi<sup>9</sup>,  
 E. M. Heenan<sup>22</sup>, I. Higuchi<sup>45</sup>, T. Higuchi<sup>46</sup>, T. Hojo<sup>32</sup>, T. Hokuue<sup>23</sup>, Y. Hoshi<sup>44</sup>,  
 S. R. Hou<sup>27</sup>, W.-S. Hou<sup>27</sup>, S.-C. Hsu<sup>27</sup>, H.-C. Huang<sup>27</sup>, T. Igaki<sup>23</sup>, Y. Igarashi<sup>9</sup>, T. Iijima<sup>23</sup>,  
 K. Inami<sup>23</sup>, A. Ishikawa<sup>23</sup>, H. Ishino<sup>47</sup>, R. Itoh<sup>9</sup>, H. Iwasaki<sup>9</sup>, Y. Iwasaki<sup>9</sup>, H. K. Jang<sup>39</sup>,  
 H. Kakuno<sup>47</sup>, J. Kaneko<sup>47</sup>, J. H. Kang<sup>55</sup>, J. S. Kang<sup>16</sup>, P. Kapusta<sup>28</sup>, S. U. Kataoka<sup>24</sup>,  
 N. Katayama<sup>9</sup>, H. Kawai<sup>3</sup>, Y. Kawakami<sup>23</sup>, N. Kawamura<sup>1</sup>, T. Kawasaki<sup>30</sup>, H. Kichimi<sup>9</sup>,  
 D. W. Kim<sup>40</sup>, Heejong Kim<sup>55</sup>, H. J. Kim<sup>55</sup>, H. O. Kim<sup>40</sup>, Hyunwoo Kim<sup>16</sup>, S. K. Kim<sup>39</sup>,  
 T. H. Kim<sup>55</sup>, K. Kinoshita<sup>5</sup>, S. Kobayashi<sup>37</sup>, P. Krokovny<sup>2</sup>, R. Kulasiri<sup>5</sup>, S. Kumar<sup>33</sup>,  
 A. Kuzmin<sup>2</sup>, Y.-J. Kwon<sup>55</sup>, J. S. Lange<sup>6,36</sup>, G. Leder<sup>12</sup>, S. H. Lee<sup>39</sup>, J. Li<sup>38</sup>, A. Limosani<sup>22</sup>,  
 D. Liventsev<sup>13</sup>, R.-S. Lu<sup>27</sup>, J. MacNaughton<sup>12</sup>, G. Majumder<sup>42</sup>, F. Mandl<sup>12</sup>, T. Matsuishi<sup>23</sup>,  
 S. Matsumoto<sup>4</sup>, T. Matsumoto<sup>23,48</sup>, Y. Mikami<sup>45</sup>, W. Mitaroff<sup>12</sup>, K. Miyabayashi<sup>24</sup>,  
 Y. Miyabayashi<sup>23</sup>, H. Miyake<sup>32</sup>, H. Miyata<sup>30</sup>, G. R. Moloney<sup>22</sup>, T. Mori<sup>4</sup>, T. Nagamine<sup>45</sup>,  
 Y. Nagasaka<sup>10</sup>, T. Nakadaira<sup>46</sup>, E. Nakano<sup>31</sup>, M. Nakao<sup>9</sup>, J. W. Nam<sup>40</sup>, Z. Natkaniec<sup>28</sup>,  
 K. Neichi<sup>44</sup>, S. Nishida<sup>17</sup>, O. Nitoh<sup>49</sup>, S. Noguchi<sup>24</sup>, T. Nozaki<sup>9</sup>, S. Ogawa<sup>43</sup>, F. Ohno<sup>47</sup>,  
 T. Ohshima<sup>23</sup>, T. Okabe<sup>23</sup>, S. Okuno<sup>15</sup>, S. L. Olsen<sup>8</sup>, W. Ostrowicz<sup>28</sup>, H. Ozaki<sup>9</sup>,  
 P. Pakhlov<sup>13</sup>, H. Palka<sup>28</sup>, C. W. Park<sup>16</sup>, H. Park<sup>18</sup>, K. S. Park<sup>40</sup>, L. S. Peak<sup>41</sup>,  
 J.-P. Perroud<sup>19</sup>, M. Peters<sup>8</sup>, L. E. Piilonen<sup>53</sup>, F. J. Ronga<sup>19</sup>, N. Root<sup>2</sup>, K. Rybicki<sup>28</sup>,  
 H. Sagawa<sup>9</sup>, S. Saitoh<sup>9</sup>, Y. Sakai<sup>9</sup>, H. Sakamoto<sup>17</sup>, M. Satpathy<sup>52</sup>, A. Satpathy<sup>9,5</sup>,  
 O. Schneider<sup>19</sup>, C. Schwanda<sup>9,12</sup>, S. Semenov<sup>13</sup>, K. Senyo<sup>23</sup>, M. E. Seviar<sup>22</sup>, H. Shibuya<sup>43</sup>,  
 M. Shimoyama<sup>24</sup>, B. Shwartz<sup>2</sup>, V. Sidorov<sup>2</sup>, J. B. Singh<sup>33</sup>, S. Stanic<sup>51,\*</sup>, A. Sugi<sup>23</sup>,  
 A. Sugiyama<sup>23</sup>, K. Sumisawa<sup>9</sup>, T. Sumiyoshi<sup>9,48</sup>, K. Suzuki<sup>9</sup>, S. Suzuki<sup>54</sup>, S. Y. Suzuki<sup>9</sup>,  
 S. K. Swain<sup>8</sup>, T. Takahashi<sup>31</sup>, F. Takasaki<sup>9</sup>, K. Tamai<sup>9</sup>, N. Tamura<sup>30</sup>, J. Tanaka<sup>46</sup>,  
 M. Tanaka<sup>9</sup>, G. N. Taylor<sup>22</sup>, Y. Teramoto<sup>31</sup>, S. Tokuda<sup>23</sup>, M. Tomoto<sup>9</sup>, T. Tomura<sup>46</sup>,  
 S. N. Tovey<sup>22</sup>, K. Trabelsi<sup>8</sup>, T. Tsuboyama<sup>9</sup>, T. Tsukamoto<sup>9</sup>, S. Uehara<sup>9</sup>, K. Ueno<sup>27</sup>,  
 Y. Unno<sup>3</sup>, S. Uno<sup>9</sup>, Y. Ushiroda<sup>9</sup>, K. E. Varvell<sup>41</sup>, C. C. Wang<sup>27</sup>, C. H. Wang<sup>26</sup>,  
 J. G. Wang<sup>53</sup>, M.-Z. Wang<sup>27</sup>, Y. Watanabe<sup>47</sup>, E. Won<sup>39</sup>, B. D. Yabsley<sup>53</sup>, Y. Yamada<sup>9</sup>,  
 A. Yamaguchi<sup>45</sup>, Y. Yamashita<sup>29</sup>, M. Yamauchi<sup>9</sup>, J. Yashima<sup>9</sup>, K. Yoshida<sup>23</sup>, Y. Yuan<sup>11</sup>,  
 Y. Yusa<sup>45</sup>, C. C. Zhang<sup>11</sup>, J. Zhang<sup>51</sup>, Z. P. Zhang<sup>38</sup>, Y. Zheng<sup>8</sup>, V. Zhilich<sup>2</sup>, Z. M. Zhu<sup>34</sup>,  
 and D. Žontar<sup>51</sup>

- <sup>1</sup>Aomori University, Aomori  
<sup>2</sup>Budker Institute of Nuclear Physics, Novosibirsk  
<sup>3</sup>Chiba University, Chiba  
<sup>4</sup>Chuo University, Tokyo  
<sup>5</sup>University of Cincinnati, Cincinnati OH  
<sup>6</sup>University of Frankfurt, Frankfurt  
<sup>7</sup>Gyeongsang National University, Chinju  
<sup>8</sup>University of Hawaii, Honolulu HI  
<sup>9</sup>High Energy Accelerator Research Organization (KEK), Tsukuba  
<sup>10</sup>Hiroshima Institute of Technology, Hiroshima  
<sup>11</sup>Institute of High Energy Physics, Chinese Academy of Sciences, Beijing  
<sup>12</sup>Institute of High Energy Physics, Vienna  
<sup>13</sup>Institute for Theoretical and Experimental Physics, Moscow  
<sup>14</sup>J. Stefan Institute, Ljubljana  
<sup>15</sup>Kanagawa University, Yokohama  
<sup>16</sup>Korea University, Seoul  
<sup>17</sup>Kyoto University, Kyoto  
<sup>18</sup>Kyungpook National University, Taegu  
<sup>19</sup>Institut de Physique des Hautes Énergies, Université de Lausanne, Lausanne  
<sup>20</sup>University of Ljubljana, Ljubljana  
<sup>21</sup>University of Maribor, Maribor  
<sup>22</sup>University of Melbourne, Victoria  
<sup>23</sup>Nagoya University, Nagoya  
<sup>24</sup>Nara Women's University, Nara  
<sup>25</sup>National Kaohsiung Normal University, Kaohsiung  
<sup>26</sup>National Lien-Ho Institute of Technology, Miao Li  
<sup>27</sup>National Taiwan University, Taipei  
<sup>28</sup>H. Niewodniczanski Institute of Nuclear Physics, Krakow  
<sup>29</sup>Nihon Dental College, Niigata  
<sup>30</sup>Niigata University, Niigata  
<sup>31</sup>Osaka City University, Osaka  
<sup>32</sup>Osaka University, Osaka  
<sup>33</sup>Panjab University, Chandigarh  
<sup>34</sup>Peking University, Beijing  
<sup>35</sup>Princeton University, Princeton NJ  
<sup>36</sup>RIKEN BNL Research Center, Brookhaven NY  
<sup>37</sup>Saga University, Saga  
<sup>38</sup>University of Science and Technology of China, Hefei  
<sup>39</sup>Seoul National University, Seoul  
<sup>40</sup>Sungkyunkwan University, Suwon  
<sup>41</sup>University of Sydney, Sydney NSW  
<sup>42</sup>Tata Institute of Fundamental Research, Bombay  
<sup>43</sup>Toho University, Funabashi  
<sup>44</sup>Tohoku Gakuin University, Tagajo  
<sup>45</sup>Tohoku University, Sendai

<sup>46</sup>University of Tokyo, Tokyo  
<sup>47</sup>Tokyo Institute of Technology, Tokyo  
<sup>48</sup>Tokyo Metropolitan University, Tokyo  
<sup>49</sup>Tokyo University of Agriculture and Technology, Tokyo  
<sup>50</sup>Toyama National College of Maritime Technology, Toyama  
<sup>51</sup>University of Tsukuba, Tsukuba  
<sup>52</sup>Utkal University, Bhubaneswer  
<sup>53</sup>Virginia Polytechnic Institute and State University, Blacksburg VA  
<sup>54</sup>Yokkaichi University, Yokkaichi  
<sup>55</sup>Yonsei University, Seoul  
\*on leave from Nova Gorica Polytechnic, Slovenia

## Abstract

We present a measurement of the electron spectrum from inclusive semileptonic  $B$  decay, using  $5.1 \text{ fb}^{-1}$  of  $\Upsilon(4S)$  data collected with the Belle detector. A high-momentum lepton tag was used to separate the semileptonic  $B$  decay electrons from secondary decay electrons. We obtained the branching fraction,  $\mathcal{B}(B \rightarrow X e^+ \nu) = (10.90 \pm 0.12 \pm 0.49)\%$ , with minimal model dependence. From this measurement, we derive a value for the Cabibbo-Kobayashi-Maskawa matrix element  $|V_{cb}| = 0.0408 \pm 0.0010(\text{exp}) \pm 0.0025(\text{th})$ .

*Key words:* CKM Matrix, semileptonic, B decay, inclusive  
*PACS numbers:* 13.20.He

## I. INTRODUCTION

The inclusive semileptonic branching fraction of  $B$  decay has long been an interesting puzzle in heavy flavor physics. Bigi et al. [1] first pointed out that theoretical calculations including QCD corrections disagreed with experimental results. While most measurements have consistently been smaller than 11% [2–4], theoretical expectations have been higher than 12%. Some theoretical analyses have been better able to accommodate a low semileptonic branching fraction by including final state mass effects in the next-to-leading order QCD corrections [5,6]. This does not necessarily solve the puzzle, however, because the semileptonic branching fraction is correlated with the rate for  $\mathcal{B}(b \rightarrow c\bar{c}s)$ , which depends on both the quark-mass ratio ( $m_c/m_b$ ) and the renormalization scale ( $\mu/m_b$ ), where  $\mu$  is used to renormalize the coupling constant ( $\alpha_s(\mu)$ ) and Wilson coefficients ( $c_{\pm}(\mu)$ ) appearing in the non-leptonic decay rate. Current measurements of the charm multiplicity in  $B$  decay ( $n_c$ ) [7] cannot easily accommodate the semileptonic branching fraction measured at the  $\Upsilon(4S)$  resonance, although measurements at higher energies [8,9] are somewhat more compatible. Further studies at the  $\Upsilon(4S)$  are needed to achieve a better understanding of  $B$  decay and theoretical models. In addition, the semileptonic branching fraction may be combined with the decay lifetime to obtain the partial width, which is used to extract the Cabibbo-Kobayashi-Maskawa (CKM) matrix element  $|V_{cb}|$  [10] and to probe theoretical models of  $B$  decay.

For this measurement, it is essential to distinguish between primary decay leptons from  $B \rightarrow X\ell^+\nu$  and secondary decay leptons produced mainly through charm decay ( $B \rightarrow \bar{D}X, \bar{D} \rightarrow Y\ell^-\bar{\nu}$ ). We have used a dilepton method introduced by ARGUS [2] to minimize model dependence in this measurement. This approach requires a high momentum lepton, an electron or a muon, to identify a  $B\bar{B}$  event and to tag the flavor of one of them. We then study the spectra of additional leptons in the event, extended to low momenta, selected so that they come mainly from decays of the other  $B$ , and separated by charge relative to the tagging lepton to distinguish primaries and secondaries effectively. This spectrum study is performed using electrons only, as their experimental identification extends to much lower momenta than that of muons. The numbers of electrons in our sample are determined by fitting the distributions of the ratio of cluster energy to track momentum ( $E/p$ ) in each kinematic bin. The branching fraction is then obtained by normalizing to the total number of tag leptons, rather than the luminosity or the number of  $B\bar{B}$  events.

In this paper, we report on the branching fraction of inclusive semileptonic  $B$  decay ( $B \rightarrow Xe^+\nu$ ) and the CKM matrix element  $|V_{cb}|$ . Charge conjugation is implicitly included. The data sample used in this analysis was collected at the  $\Upsilon(4S)$  resonance with the Belle detector [11] at the KEKB asymmetric  $e^+e^-$  (3.5 on 8 GeV) collider [12]. This analysis is based on an integrated luminosity of  $5.1 \text{ fb}^{-1}$  at the  $\Upsilon(4S)$  resonance, and  $0.6 \text{ fb}^{-1}$  continuum data at a center-of-mass energy of 60 MeV below the  $\Upsilon(4S)$ . A GEANT [13] based Monte Carlo simulation was used to model the detector response.

## II. THE BELLE DETECTOR

The Belle detector is configured around a 1.5 T superconducting solenoid and iron structure surrounding the KEKB interaction region. It covers 92% of the total solid angle in the

$\Upsilon(4S)$  center-of-mass (CM) system. Charged-particle tracking is provided by three layers of double-sided silicon vertex detectors (SVD) and a 50-layer central drift chamber (CDC). Eighteen of the wire layers provide a small stereo angle to measure the coordinates of the particle trajectories in the direction of the beam ( $z$ ). The transverse momentum resolution for charged tracks is  $(\sigma_{p_t}/p_t)^2 = (0.0019p_t)^2 + (0.0030)^2$ , where  $p_t$  is in GeV/ $c$ .

Charged hadron identification is provided by  $dE/dx$  measurements in the CDC, an aerogel Čerenkov counter (ACC), and a time-of-flight scintillation counter (TOF). The  $dE/dx$  measurements have a resolution for lepton tracks of 6% and are useful for separating electrons from hadrons over nearly the full momentum range. The ACC and the TOF are used to reject charged  $K$  and proton tracks.

The electromagnetic calorimeter (ECL) contains 8736 CsI(Tl) crystals located behind the hadron identification detectors, inside the solenoid. Its thickness is 16.2 radiation lengths over the entire tracking acceptance. The photon energy resolution is  $(\sigma_E/E)^2 = (0.013)^2 + (0.0007/E)^2 + (0.008/E^{1/4})^2$ , where  $E$  is in GeV.

The  $\mu/K_L$  detector (KLM) located outside the coil consists of 15 sensitive layers and 14 iron layers in the octagonal barrel region. The iron plates and associated materials provide a total of 4.7 nuclear interaction lengths at normal incidence.

### III. DILEPTON SELECTION

Hadronic events were selected based on charged track information from the CDC and cluster information from the ECL after transformation to the CM system. We required at least three charged tracks, an energy sum in the calorimeter between 10% and 80% of  $\sqrt{s}$ , a total energy sum of greater than 20% of  $\sqrt{s}$ , and a total momentum balanced in the  $z$  direction within 2.1 GeV/ $c$ . This removed the majority of two-photon, radiative Bhabha, and  $\tau^+\tau^-$  events where both  $\tau$ 's decay to leptons. Remaining radiative Bhabha events were removed by requiring at least two large angle clusters in the ECL and that the average cluster energy be below 1 GeV. In order to remove higher multiplicity  $\tau^+\tau^-$  events, we calculated the invariant mass of the particles found in each hemisphere perpendicular to the event thrust axis and removed the event if it fell below the  $\tau$  mass. Beam-gas and beam-wall backgrounds were removed by reconstructing the primary vertex of the event and requiring it to be consistent with the known location of the interaction point(IP). To suppress continuum, we required that the ratio  $R_2$  of second to zeroth Fox-Wolfram moments [14] be less than 0.6.

Events containing a high-momentum “tagging lepton” to tag the  $B$  flavor and a “spectrum electron” for the spectrum study were selected from the hadronic event sample. To select tagging electrons, we used  $dE/dx$  measurements in the CDC, the response of the ACC, matching between the ECL cluster and associated CDC track, the shower shape of the ECL cluster, and  $E/p$ , the ratio of the ECL energy to the momentum of the associated CDC track. Each set of measurements was translated into an electron probability. These probabilities were then combined into a single likelihood discriminant,  $L_e$ . For the selection of tagging muons, we defined an equivalent likelihood discriminant  $L_\mu$  from information on the location and penetration depth of the associated track in the KLM. In addition to the requirements  $L_e > 0.8$  and  $L_\mu > 0.95$ , the tagging lepton tracks were required to satisfy  $1.4 \text{ GeV}/c < p < 2.2 \text{ GeV}/c$ ,  $45^\circ < \theta_{\text{lab}} < 125^\circ$ ,  $|dr_{IP}| < 0.2 \text{ cm}$ , and  $|dz_{IP}| < 10 \text{ cm}$ , where

$p$  is the CM momentum,  $\theta_{\text{lab}}$  is the polar angle of the track in the laboratory frame, and  $dz_{IP}$  and  $dr_{IP}$  are the distances of closest approach to the IP in the direction of the beam and in the plane perpendicular to it, respectively. For tagging electrons that satisfy the above selection criteria, the detection efficiency, determined by embedding single simulated tracks in multi-hadron data, is 92%, and the misidentification probability for hadrons, determined from  $K_S^0 \rightarrow \pi^+\pi^-$  decays, is less than 0.4%. For tagging muons, the efficiency and misidentification probability, determined in a similar way, are 86% and 1.2%, respectively.

To select electron candidates for the spectrum measurement, we required that tracks satisfy  $p_{\text{lab}} > 0.5 \text{ GeV}/c$ ,  $46^\circ < \theta_{\text{lab}} < 125^\circ$ ,  $|dr_{IP}| < 0.3 \text{ cm}$  and  $|dz_{IP}| < 4.0 \text{ cm}$  ( $p_{\text{lab}}$  is the momentum in the laboratory frame). We used  $dE/dx$ , TOF, and ACC information to reject tracks that are strongly identified as being other than electrons by a likelihood criterion of  $L_{\text{non-}e} < 0.95$ . The efficiency of this cut for retaining electrons was 98.6%. We did not use ECL cluster information because that was used at a later stage to extract electron yields by fitting the  $E/p$  distribution.

Further requirements were made to reduce backgrounds from several known sources. Events were rejected if any track satisfying the lepton identification requirement of  $L_e > 0.8$  or  $L_\mu > 0.95$  could be paired with any other oppositely charged track to obtain an invariant mass within  $50 \text{ MeV}/c^2$  of the  $J/\psi$  mass. To remove electrons originating from  $\gamma$  conversions, we rejected all pairs of oppositely-charged tracks where at least one track satisfied  $L_e > 0.8$  and the  $e^+e^-$  invariant mass was less than  $0.10 \text{ GeV}/c^2$ . To remove electrons from  $\pi^0$  Dalitz decays, oppositely charged track pairs with  $e^+e^-$  invariant mass less than  $0.10 \text{ GeV}/c^2$  were combined with photon candidates and rejected if the  $e^+e^-\gamma$  invariant mass of any combination was consistent with the  $\pi^0$  mass.

To reduce dileptons in continuum events, which tend to be back-to-back, and ‘‘ghost’’ tracks (one track mis-reconstructed as two nearly collinear tracks), we required  $-0.8 < \cos\theta_{\ell e} < 0.998$  for both opposite-sign and same-sign dileptons, where  $\theta_{\ell e}$  is the opening angle between the tagging lepton and the spectrum electron in the CM frame.

To reject same- $B$  backgrounds, where both leptons originate from just one  $B$  meson, we look at angular, kinematic, and charge correlations. The spectrum electron and the tagging lepton, if correctly selected, have opposite charges unless one of the parent  $B$  mesons has mixed. If a secondary electron is selected as the spectrum electron, the charge combination is opposite to the above case. If a secondary electron from the same  $B$  as the tagging lepton is selected as the spectrum electron, it has a charge opposite to that of the tagging lepton. Opposite-sign dileptons were required to satisfy either  $p_e + \cos\theta_{\ell e} > 1.2$  ( $p_e$  in  $\text{GeV}/c$ ) or  $\cos\theta_{\ell e} > 0.3$ . This criterion reduced the fraction of the same- $B$  background in the spectrum electron candidates to 2% while retaining 61% of the signal.

#### IV. SIGNAL YIELD AND BACKGROUND SUBTRACTION

To extract the number of dilepton events from the lepton-tagged events, a maximum likelihood fit was performed on the  $E/p$  distributions of the spectrum electron candidates in each momentum ( $p$ ) and polar angle ( $\theta_{\text{lab}}$ ) bin as shown in Fig. 1, where the momentum range is divided into 46 bins of width  $0.05 \text{ GeV}/c$  ( $0.5\text{--}2.8 \text{ GeV}/c$ ), the polar angle region is divided into 4 bins ( $46\text{--}60^\circ$ ,  $60\text{--}78^\circ$ ,  $78\text{--}97^\circ$  and  $97\text{--}125^\circ$ ), and same- and opposite-sign dileptons are treated separately. The signal probability density function (PDF) was obtained

using  $e^+$  and  $e^-$  from photon conversions and from the two-photon process. The background PDF was taken from the sample of tracks rejected by the electron identification requirements for the spectrum study. By determining both signal and background PDF's in the same bins of momentum and angle as the dilepton sample, we removed any systematic effects due to differences in momentum and angular distribution between the samples used to obtain the PDF's and our dilepton sample.

The raw momentum spectra in the CM frame for both opposite-sign and same-sign electrons with the above selections applied are shown in Fig. 2. The total yields were  $19722 \pm 147$  opposite-sign (OS) and  $11224 \pm 117$  same-sign (SS) dileptons in the data taken at the  $\Upsilon(4S)$ , and  $791 \pm 105$  OS and  $448 \pm 87$  SS below resonance (after scaling). The raw yields are shown in Table I. The continuum contribution was subtracted by scaling the dilepton yields in the off-resonance data. The scaling factor is the ratio of the on- and off-resonance integrated luminosity, after correcting for the energy dependence of the continuum cross section.

These uncorrected spectra contain several backgrounds that are accounted for and subtracted. Leptons from  $J/\psi$  decay and electrons from  $\gamma$  conversion and  $\pi^0$  Dalitz decays can survive when one of the pair has escaped detection. These backgrounds are determined by Monte Carlo simulation, and the uncertainties were evaluated from the error on each rate. Contributions from previously unaccounted sources of secondary leptons from  $B$  decay were modeled via Monte Carlo, assuming current values of branching fractions:  $B \rightarrow X\tau^+\nu, \tau^+ \rightarrow e^+Y$  ( $\mathcal{B}(B \rightarrow X\tau^+\nu) = (2.6 \pm 0.4)\%$  [16]),  $B \rightarrow D_s X, D_s \rightarrow e^-Y$  ( $\mathcal{B}(B \rightarrow D_s X)\mathcal{B}(D_s \rightarrow e^-Y) = (0.8 \pm 0.3)\%$ ),  $B \rightarrow \Lambda_c X, \Lambda_c \rightarrow e^+Y$  ( $\mathcal{B}(B \rightarrow \Lambda_c X)\mathcal{B}(\Lambda_c \rightarrow e^+Y) = (0.29 \pm 0.12)\%$ ),  $B \rightarrow DX_{\bar{c}}, D \rightarrow Ye^+\nu$  via  $\bar{b} \rightarrow \bar{c}c\bar{s}$  ( $\mathcal{B}(B \rightarrow DX_{\bar{c}}) = (7.9 \pm 2.2)\%$  [15]). False tag leptons arise mainly from secondary leptons and fake muons, whose contamination was estimated to be  $(2.2 \pm 0.4)\%$  and  $(1.5 \pm 0.8)\%$ , respectively. All backgrounds in the dilepton events were scaled by normalizing to the number of lepton-tagged events. The background yields and their errors are summarized in Table I. The spectra of the total  $B\bar{B}$  backgrounds are included in Fig. 2.

## V. MEASUREMENT OF BRANCHING FRACTION

The opposite- and same-sign electron spectra after background corrections can be written as

$$\frac{dN_{+-}}{dp} = \epsilon_{k1}(p)\eta(p)N_{\text{tag}} \left[ \frac{d\mathcal{B}(B \rightarrow Xe^+\nu)}{dp}(1 - \chi) + \frac{d\mathcal{B}(B \rightarrow \bar{D}X, \bar{D} \rightarrow Ye^-\bar{\nu})}{dp}\chi \right], \quad (1)$$

$$\frac{dN_{\pm\pm}}{dp} = \epsilon_{k2}(p)\eta(p)N_{\text{tag}} \left[ \frac{d\mathcal{B}(B \rightarrow Xe^+\nu)}{dp}\chi + \frac{d\mathcal{B}(B \rightarrow \bar{D}X, \bar{D} \rightarrow Ye^-\bar{\nu})}{dp}(1 - \chi) \right], \quad (2)$$

where  $N_{\text{tag}}$  is the number of tag leptons,  $\eta(p)$  is the electron identification efficiency as a function of the momentum, which also includes the momentum smearing effect from bremsstrahlung, and  $\epsilon_k(p)$  is the efficiency of our kinematic selection, determined from a Monte Carlo simulation.  $\chi$  is an effective mixing parameter for all  $B$  mesons coming from  $\Upsilon(4S)$  decay,  $\chi \equiv \chi_0 f_{00}$ , where  $\chi_0$  is the fraction of neutral  $B$  events decaying as mixed ( $B^0 B^0$  or  $\bar{B}^0 \bar{B}^0$ ) and  $f_{00}$  ( $f_{+-}$ ) is the branching fraction for  $\Upsilon(4S)$  decay

into  $B^0\bar{B}^0(B^+B^-)$ . We used  $\chi = 0.0853 \pm 0.0055$ , calculated using  $\chi_0 = 0.174 \pm 0.009$ ,  $f_{+-}/f_{00} = 1.04 \pm 0.08$  [16], and  $f_{+-} + f_{00} = 1.0$ . The two spectra,  $d\mathcal{B}(B \rightarrow Xe^+\nu)/dp$  and  $d\mathcal{B}(B \rightarrow \bar{D}X, \bar{D} \rightarrow Ye^-\bar{\nu})/dp$ , can be obtained from the measured  $dN_{+-}/dp$  and  $dN_{\pm\pm}/dp$  spectra by solving equations (1) and (2) simultaneously.

The number of tags was determined by counting leptons above 1.4 GeV/ $c$ , subtracting backgrounds, and correcting for the relative efficiency for selecting dilepton events compared to single-lepton events [(94.8 $\pm$ 0.5)%]. As a consequence, we found the number of tags to be  $N_{\text{tag}} = 528975 \pm 1412(\text{stat})$ . The difference in the relative efficiency between opposite-sign and same-sign dilepton events was also corrected for in each electron spectrum.

By solving the equations, we obtained the momentum spectra for both the primary and secondary electrons, as shown in Fig. 3. The primary electron spectrum was integrated from 0.6 to 2.8 GeV/ $c$  to extract the partial branching fraction for semileptonic  $B$  decay,

$$\mathcal{B}(B \rightarrow Xe^+\nu \mid p > 0.6 \text{ GeV}/c) = (10.24 \pm 0.11(\text{stat}) \pm 0.46(\text{syst}))\%. \quad (3)$$

The relative size of the undetected region of the electron spectrum was studied using the ACCMM [17] and ISGW2 [18] models and a semi-empirical shape [19] for  $b \rightarrow c$  decay, with options to include semileptonic decay with baryons [19], and charmless semileptonic  $B$  decays. As part of our evaluation, we fitted the measured primary spectrum to the prediction of each model. Results of the fitting are shown in Table II. For all models, the fits were improved when the proportion of decays  $B \rightarrow D^{**}\ell\nu$  was allowed to float to higher values than were nominally set in the model. We obtained the best  $\chi^2$  fit using a semi-empirical shape, with  $\mathcal{B}(B \rightarrow X_u e\nu)$  fixed to 0.167%, and the following quantities allowed to vary (fitted values with statistical error are shown):  $\mathcal{B}(B \rightarrow D^{(*)}e\nu) = 7.31 \pm 0.28\%$ ,  $\mathcal{B}(B \rightarrow D^{**}e\nu) = 2.51 \pm 1.00\%$ ,  $\mathcal{B}(B \rightarrow D^{(*)}\pi e\nu) = 0.78 \pm 0.96\%$  and  $\mathcal{B}(B \rightarrow \text{baryons } e\nu) = 0.03 \pm 0.31\%$ . We extrapolated the branching fraction below 0.6 GeV/ $c$  using the electron momentum spectrum of this “best-fit” model. We found that the extrapolated area was (6.1 $\pm$ 0.7)% of the total decay width, where the error was taken from the largest difference between the best-fit model and the other models (excepting ACCMM, which gave a poor fit). We obtained:

$$\mathcal{B}(B \rightarrow Xe^+\nu) = (10.90 \pm 0.12(\text{stat}) \pm 0.49(\text{syst}))\%. \quad (4)$$

This result is consistent with other measurements [3,4].

To determine the CKM matrix element  $|V_{cb}|$  we first subtracted the contribution from charmless decay ( $\mathcal{B}(B \rightarrow X_u \ell\nu) = (0.167 \pm 0.055)\%$ ) and assumed  $\mathcal{B}(B \rightarrow Xe^+\nu) = \mathcal{B}(B \rightarrow X\ell\nu)$ . Using a formula based on the heavy quark expansion [20], with  $\mu_\pi^2 = (0.5 \pm 0.2) \text{ GeV}^2$ ,  $m_b = 4.58 \pm 0.05 \text{ GeV}/c^2$  and the world-average value for  $B$  lifetime,  $\tau_B = 1.607 \pm 0.021 \text{ ps}$  (average of  $B^0$  and  $B^+$ ) [16], our evaluation is

$$|V_{cb}| = 0.0408 \pm 0.0010(\text{exp}) \pm 0.0025(\text{th}), \quad (5)$$

where the first error includes both the statistical and systematic uncertainties and the second error arises from theoretical uncertainties.

The branching fraction for secondary decay,  $\mathcal{B}(B \rightarrow \bar{D}X, \bar{D} \rightarrow Ye^-\bar{\nu})$ , was extracted by fitting the secondary electron spectrum to the ACCMM and ISGW2 model predictions. We found

$$\begin{aligned}
\mathcal{B}(B \rightarrow \bar{D}X, \bar{D} \rightarrow Ye^{-}\bar{\nu}) &= (7.06 \pm 0.14(\text{stat}) \pm 0.48(\text{syst}))\% \text{ (ACMM)} \\
&= (7.84 \pm 0.13(\text{stat}) \pm 0.48(\text{syst}))\% \text{ (ISGW2)}
\end{aligned}
\tag{6}$$

The obtained branching fraction of the secondary charm semileptonic decay is consistent with results from other experiments [15,16].

## VI. SYSTEMATIC ERRORS

The systematic uncertainties on  $\mathcal{B}(B \rightarrow Xe^{+}\nu)$  and  $\mathcal{B}(B \rightarrow \bar{D}X, \bar{D} \rightarrow Ye^{-}\bar{\nu})$  are summarized in Table III. The main contributions are the uncertainties in the tracking and identification efficiencies for the electrons used in the spectrum study. The tracking efficiency was estimated by embedding electron tracks into hadronic event data and repeating the tracking procedures to evaluate the efficiency of the embedded electron. The embedded electrons were obtained from single electron Monte Carlo as well as from electrons in two-photon data. The tracking efficiency was also estimated by embedding into simulated  $B\bar{B}$  events, and the absolute difference in values from the two methods was taken as the uncertainty.

The electron identification included two steps: hadron-muon rejection and  $E/p$  fitting. The inefficiency in the first step (1.4%) was found from a study using photon conversion electrons embedded into hadronic events in data. The systematic uncertainty of 0.8% on this effect was estimated by taking the difference between results obtained from embedding in data and MC. Uncertainties in  $E/p$  fitting can come from impurities in the data samples used to obtain the signal and background shapes as well as differences in the event environment between those data samples and dileptons. The signal shapes were obtained from photon conversion electrons in the hadronic sample and two photon data, while the background shapes were obtained from tracks failing the hadron-muon rejection. Impurities in these samples were estimated via Monte Carlo, and systematic uncertainties of 0.9% and 0.8% were assigned for fitting of electron and hadron shapes, respectively. The uncertainty due to differences in event environment was also estimated using MC and found to be 1.3%. The quadratic sum of the contributions gives a net uncertainty on electron identification of 2.0%.

The uncertainty in the kinematic selection efficiency was estimated by changing the event selection criteria for signal events. Instead of requiring either  $p_e + \cos\theta_{\ell e} > 1.2$  or  $\cos\theta_{\ell e} > 0.3$ , we required either  $p_e + \cos\theta_{\ell e} > 1.0$  or  $\cos\theta_{\ell e} > 0$ . We also varied the polar angle region for tag leptons and considered the ranges;  $45^\circ < \theta_{\text{lab}} < 65^\circ$ ,  $65^\circ < \theta_{\text{lab}} < 90^\circ$  and  $90^\circ < \theta_{\text{lab}} < 125^\circ$ . The maximum deviation of the results was assigned to a systematic error.

The systematic uncertainty in the continuum subtraction was attributed to the uncertainty on the normalization between on-resonance and off-resonance. The uncertainty was estimated from the error on the integrated luminosity. This effect is larger for the lepton tag events than the dilepton events since the fraction of continuum background for tag events is much higher than for dilepton events.

There were two contributions to the uncertainty on the background subtraction in the dilepton events. The first is the uncertainties on the branching fractions of the various sources, which are given in Section IV. The second is the uncertainty on the scale factor used to normalize background yields obtained from Monte Carlo simulation. The dominant

contributor to this effect is the uncertainty in the number of tag leptons, which was used to determine scaling factors.

The main sources for the uncertainty on the relative efficiency are the invariant mass cuts to reject electrons from  $J/\psi$  and gamma conversions. This uncertainty was estimated by taking the difference of the final yields with and without the cuts.

## VII. CONCLUSION

In conclusion, we have measured the branching fraction for inclusive semileptonic  $B$  decay using a high-momentum lepton tag. The result is

$$\mathcal{B}(B \rightarrow X e^+ \nu) = (10.90 \pm 0.12 \pm 0.49)\%, \quad (7)$$

where the first error is statistical and the second is systematic. This result agrees with other measurements. From this result and the world average  $B$  meson lifetime [16], we have extracted the CKM parameter  $|V_{cb}|$  as follows:

$$|V_{cb}| = 0.0408 \pm 0.0010(\text{exp}) \pm 0.0025(\text{th}). \quad (8)$$

## ACKNOWLEDGMENTS

We wish to thank the KEKB accelerator group for the excellent operation of the KEKB accelerator. We acknowledge support from the Ministry of Education, Culture, Sports, Science, and Technology of Japan and the Japan Society for the Promotion of Science; the Australian Research Council and the Australian Department of Industry, Science and Resources; the National Science Foundation of China under contract No. 10175071; the Department of Science and Technology of India; the BK21 program of the Ministry of Education of Korea and the CHEP SRC program of the Korea Science and Engineering Foundation and the Center for High Energy Physics sponsored by the KOSEF and the Yonsei University Faculty Research Support program; the Polish State Committee for Scientific Research under contract No. 2P03B 17017; the Ministry of Science and Technology of the Russian Federation; the Ministry of Education, Science and Sport of the Republic of Slovenia; the National Science Council and the Ministry of Education of Taiwan; and the U.S. Department of Energy.

TABLE I. Yield of electrons with momentum of  $0.6 \text{ GeV}/c < p_e < 2.8 \text{ GeV}/c$  in lepton-tagged events. The background yields and their statistical errors were determined by a Monte Carlo simulation. The second errors are due to branching fraction uncertainties.

	Opposite sign	Same sign
On-resonance data	$19722 \pm 147$	$11224 \pm 117$
Scaled off-resonance	$791 \pm 105$	$448 \pm 87$
Continuum subtracted	$18931 \pm 181$	$10776 \pm 146$
Lepton from $J/\psi$ or $\psi'$	$167 \pm 8 \pm 33$	$179 \pm 8 \pm 36$
$e$ from $\gamma$	$127 \pm 7 \pm 32$	$306 \pm 10 \pm 77$
$e$ from $\pi^0, \eta$	$30 \pm 3 \pm 8$	$88 \pm 6 \pm 22$
$e$ from $\tau$	$406 \pm 12 \pm 84$	$75 \pm 5 \pm 16$
$e$ from $\Lambda_c$	$8 \pm 2 \pm 3$	$177 \pm 8 \pm 71$
$e$ from $D_s$	$293 \pm 10 \pm 88$	$64 \pm 5 \pm 19$
$e$ from $D(B \rightarrow DX)$	$285 \pm 10 \pm 86$	$54 \pm 4 \pm 16$
Same- $B$	$397 \pm 12 \pm 79$	—
Tag from $D$	$160 \pm 8 \pm 32$	$600 \pm 15 \pm 120$
Fake lepton tags	$240 \pm 9 \pm 120$	$323 \pm 11 \pm 162$
Other backgrounds	$43 \pm 4 \pm 13$	$51 \pm 4 \pm 15$
Total background	$2156 \pm 28 \pm 215$	$1917 \pm 26 \pm 233$
Background subtracted	$16775 \pm 183 \pm 215$	$8859 \pm 148 \pm 233 \pm 148 \pm 233$

TABLE II. Goodness-of-fit for various models fitted to the primary spectrum. Models modified to vary the fraction of  $D^{**}$  are indicated by '\*\*', and the “best fit” is described in the text.

Model	$\chi^2/DOF$
QQ98 [19]	50.0/43
ISGW2 [18]	70.0/43
ISGW	48.3/43
ACCMM [17]	125.8/43
ISGW2**	32.5/41
QQ98 **	30.2/42
QQ98 (best fit)	28.4/39

TABLE III. Summary of systematic errors on the branching fractions.

Source of uncertainty	$\frac{\Delta\mathcal{B}}{\mathcal{B}}(B \rightarrow X e^+ \nu)$ (%)	$\frac{\Delta\mathcal{B}}{\mathcal{B}}(B \rightarrow \bar{D} X, \bar{D} \rightarrow Y e^- \bar{\nu})$ (%)
Tracking	2.9	2.9
Electron identification	2.0	2.0
Kinematic selection	1.4	4.1
Continuum subtraction	0.7	0.9
Background subtraction	1.8	2.3
Mixing parameter	0.6	1.5
Relative efficiency	1.3	0.8
Model prediction	0.7	10.4
Total	4.5	12.1

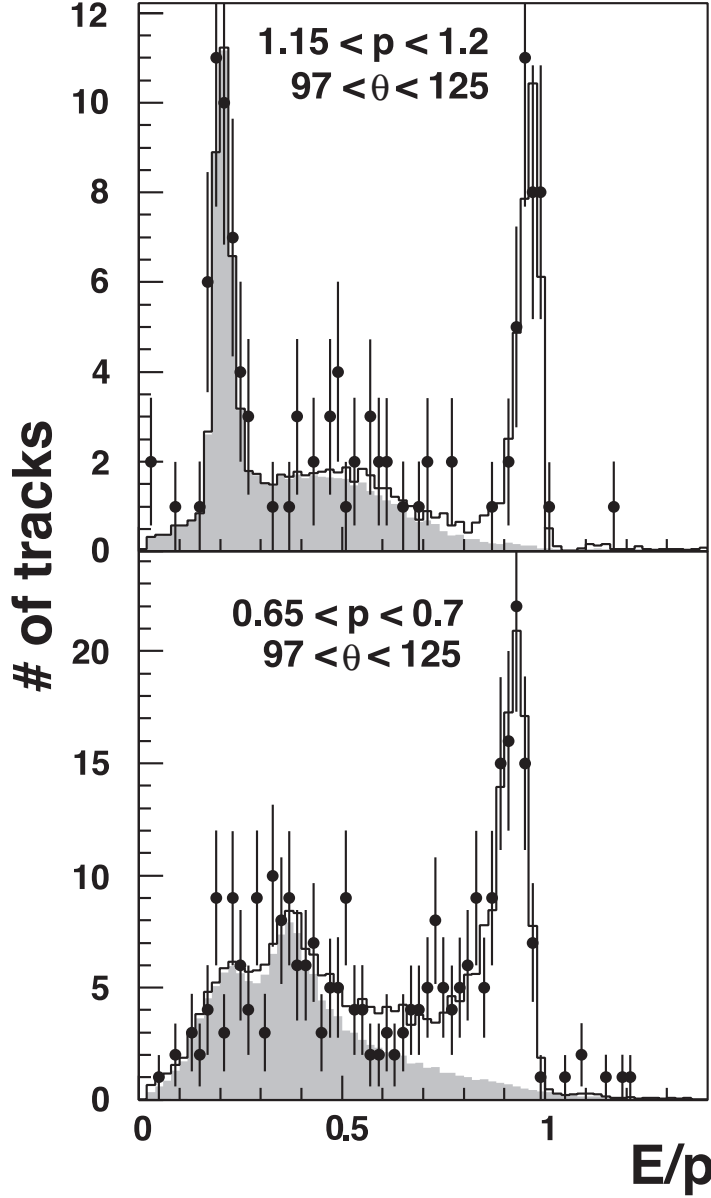


FIG. 1.  $E/p$  distributions for electron candidates in the momentum ranges 1.15–1.2 GeV/ $c$  (top) and 0.65–0.7 GeV/ $c$  (bottom) with the electron candidate track in the polar angle range between  $97^\circ$  and  $125^\circ$  in the laboratory frame. The points with error bars are the data, the solid histogram is the sum of signal and background components, and the shaded area shows the non-electron background contribution.

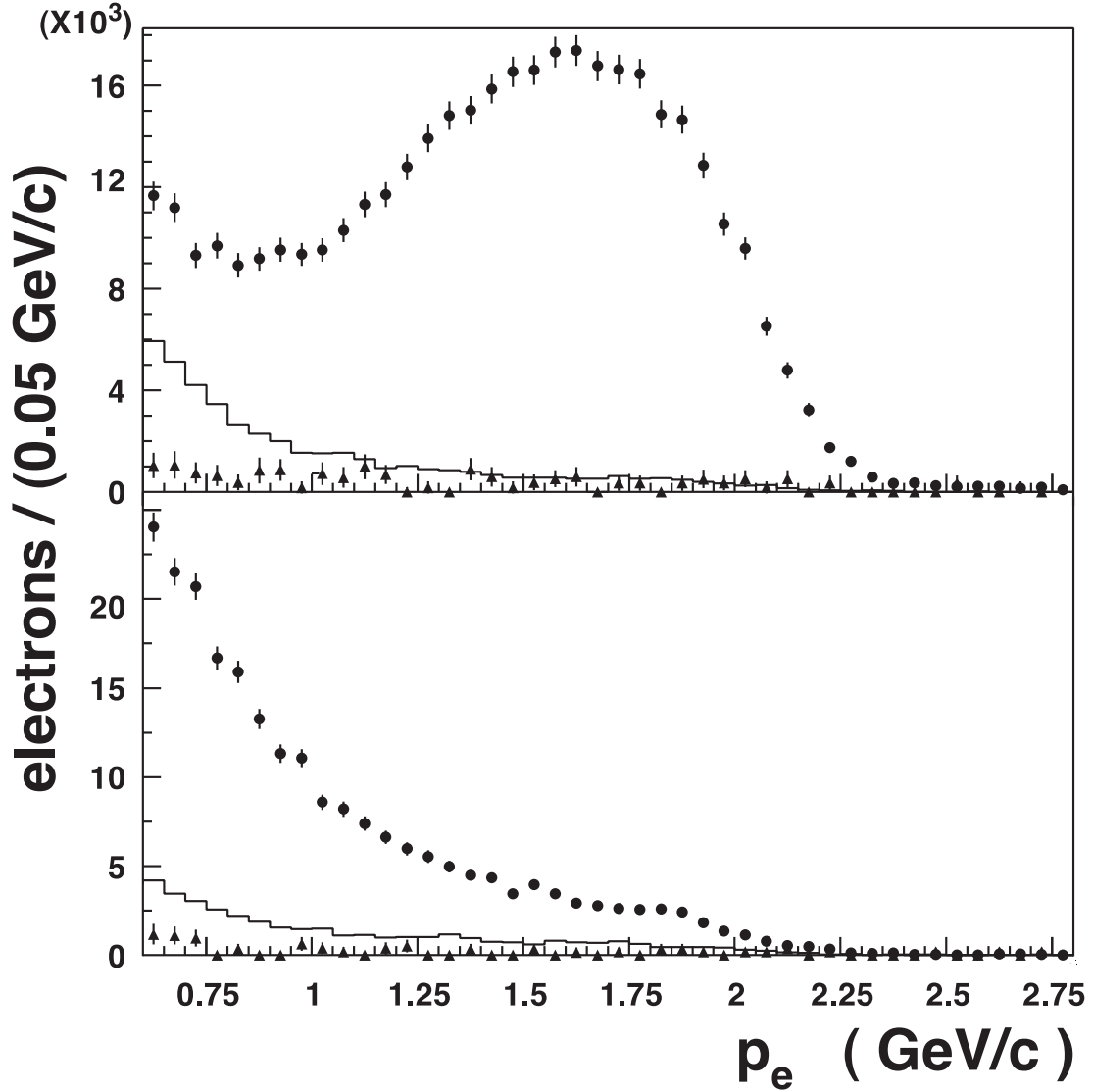


FIG. 2. Electron momentum spectra. The top and bottom figures show the spectra of opposite-sign and same-sign electrons, respectively. The closed circles are the on-resonance data. The triangles show the scaled off-resonance data. The error bars indicate only the statistical error. The histogram is the MC-determined  $B\bar{B}$  background.

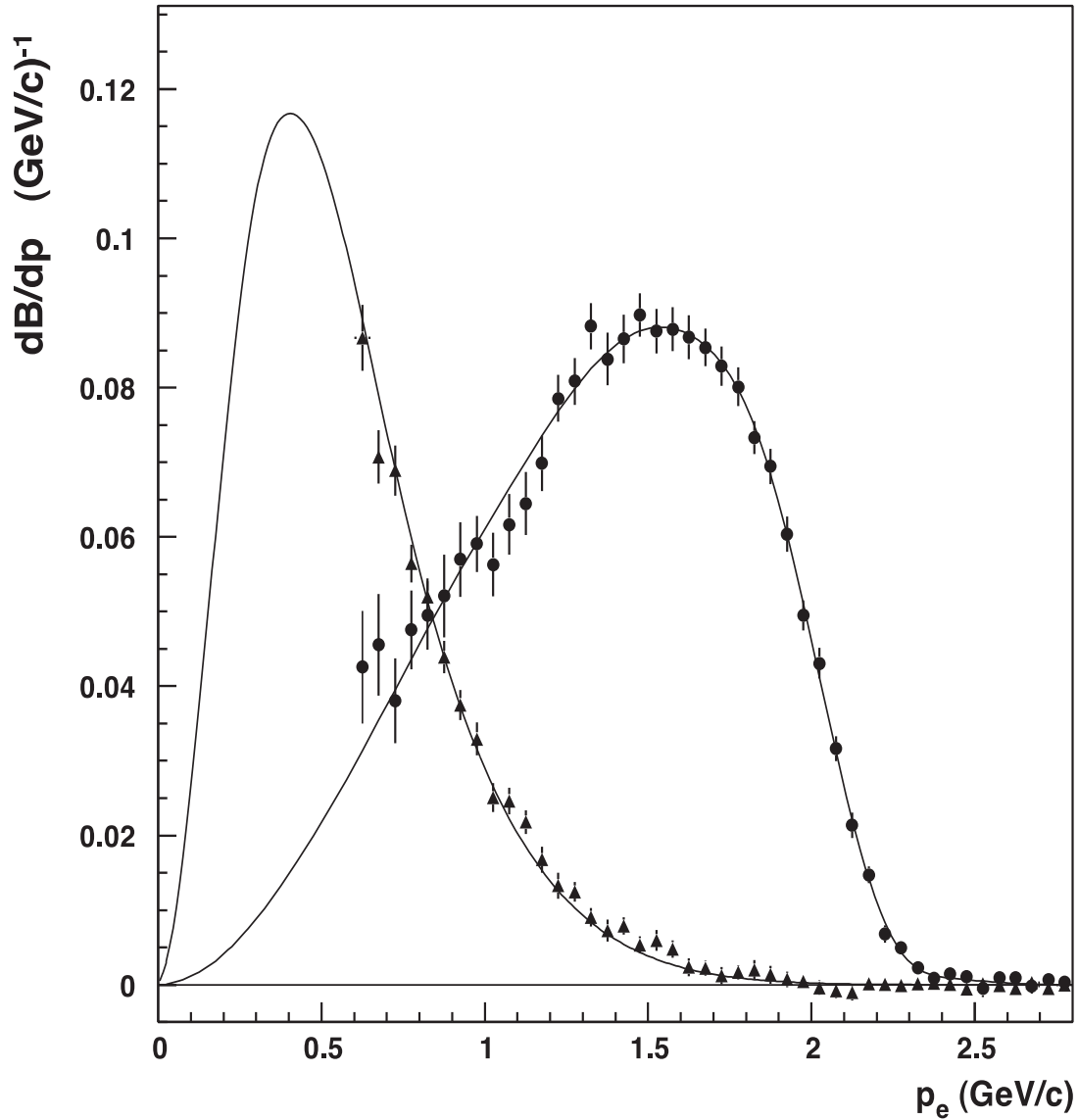


FIG. 3. Final results for the electron spectra of primary (circles) and secondary (triangles) semileptonic decays. The solid curve superimposed on the primary electron spectrum is the best-fit model described in the text, while the curve for the secondary electron spectrum is the ISGW2 model.

## REFERENCES

- [1] I. Bigi, B. Blok, M. Shifman, A. Vainshtein, Phys. Lett. **B323** (1994) 408.
- [2] ARGUS Collaboration, H. Albrecht *et al.*, Phys. Lett. **B318** (1993) 397.
- [3] CLEO Collaboration, B. Barish *et al.*, Phys. Rev. Lett. **76** (1997) 1570.
- [4] ALEPH Collaboration, D. Buskulic *et al.*, Z. Phys. **C62** (1994) 179;  
 DELPHI Collaboration, P. Abreu *et al.*, Z. Phys. **C66** (1995) 323;  
 L3 Collaboration, M. Acciarri *et al.*, Z. Phys. **C71** (1996) 379;  
 OPAL Collaboration, G. Abbiendi *et al.*, Eur. Phys. J. **C13** (2000) 225;  
 L3 Collaboration, M. Acciarri *et al.*, Eur. Phys. J. **C13** (2000) 47;  
 ALEPH, CDF, DELPHI, L3, OPAL, and SLD Collaborations,  
 D. Abbaneo *et al.*, SLAC-PUB-8492, CERN-EP-2000-096,  
 this paper indicates that  $\mathcal{B}(b \rightarrow xlv)$  is  $(10.58 \pm 0.07 \pm 0.17)\%$ .
- [5] A. F. Falk, M. B. Wise, I. Dunietz, Phys. Rev. **D51** (1995) 1183;  
 E. Bagan, Patricia Ball, V. M. Braun, P. Gosdzinsky, Nucl. Phys. **B432** (1994) 3;  
 E. Bagan, Patricia Ball, V. M. Braun, P. Gosdzinsky, Phys. Lett. **B342** (1995) 362;  
 erratum, Phys. Lett. **B374** (1996) 363;  
 M. B. Voloshin, Phys. Rev. **D51** (1995) 3948.
- [6] M. Neubert and C. T. Sachrajda, Nucl. Phys. **B483** (1997) 339.
- [7] CLEO Collaboration, L. Gibbons *et al.*, Phys. Rev. **D56** (1997) 3783.
- [8] DELPHI Collaboration, P. Abreu *et al.*, Phys. Lett. **B426** (1998) 193.
- [9] ALEPH Collaboration, D. Buskulic *et al.*, Phys. Lett. **B388** (1996) 648.
- [10] M. Kobayashi and T. Maskawa, Prog. Theor. Phys. **49** (1973) 652;  
 N. Cabibbo, Phys. Rev. Lett. **10** (1963) 531.
- [11] BELLE Collaboration, A. Abashian *et al.*, Nucl. Inst. and Meth. **A479** (2002) 117.
- [12] E Kikutani ed., KEK Preprint 2001-157 (2001), to appear in Nucl. Instr. and Meth. A.
- [13] R. Brun *et al.*, GEANT 3.21, CERN Report No. DD/EE/84-1 (1987).
- [14] G. Fox and S. Wolfram, Phys. Rev. Lett **41** (1978) 1581.
- [15] CLEO Collaboration, T. E. Coan, *et al.*, Phys. Rev. Lett **80** (1998) 1150.
- [16] Particle Data Group, Eur. J. **C15** (2000) 1.
- [17] G. Altarelli, N. Cabibbo, G. Corbo, L. Maiani, G. Martinelli, Nucl. Phys. **B208** (1982) 365.
- [18] N. Isgur, D. Scora, B. Grinstein, M. B. Wise, Phys. Rev. **D39** (1989) 799;  
 D. Scora, N. Isgur, Phys. Rev. **D52** (1995) 2783.
- [19] ‘QQ - The CLEO Event Generator’,  
<http://www.lns.cornell.edu/public/CLEO/soft/qq> (unpublished).
- [20] I. Bigi, preprint hep-ph/9907270;  
 I. Bigi, M. Shifman, N. Uraltsev, Ann. Rev. Nucl. Part. Sci. **47** (1997) 591.